JOURNAL OF MATERIALS SCIENCE 28 (1993) 5800–5808

Structures and properties of $La_{1-x}Sr_xCoO_{3-y}$ prepared by freeze drying

J. KIRCHNEROVA*, D. B. HIBBERT
Department of Analytical Chemistry, University of New South Wales, P.O. Box 1, Kensington, New South Wales 2033, Australia

Several samples of $La_{1-x}Sr_xCoO_{3-y}$ ($x = 1$, 0.8, 0.5, 0.2) were prepared by calcining freeze-dried, stoichiometric mixtures of nitrates at different temperatures and for different lengths of time. Selected samples were characterized by powder X-ray diffraction, conductivity measurements, Brunauer–Emmett–Teller surface area measurement, and by electrochemical cyclic voltammetry in alkaline solutions and alkaline solutions containing methanol. The structures of each composition were complex and varied with composition and preparation conditions. There is evidence for non-stoichiometry caused by oxygen anion vacancies. For $La_{0.5}Sr_{0.5}CoO_{3-y}$ the electrochemical activity towards the oxidation of methanol is a maximum at the fully formed cubic perovskite. The oxidation currents at $La_{0.8}Sr_{0.2}CoO_{3-y}$ and $La_{0.2}Sr_{0.8}CoO_{3-y}$ go through maxima at more distorted structures.

1. Introduction

Perovskites based on strontium-doped lanthanum cobalt oxide $La_{1-x}Sr_xCoO_3$ have been studied for many years [1–3] and continue to attract interest for their catalytic properties and their usefulness as model systems that are easily prepared [4–7]. Many perovskites are metallic, have high catalytic activity, high heat resistance, high electrical conductivity and unusual magnetic properties. To this class of compounds belong the recently discovered copper-based oxides showing a high superconducting transition temperature [8]. These latter compounds have renewed the debate concerning anion vacancies and the importance of non-stoichiometry. The structure of the series of compounds of stoichiometry $La_{1-x}Sr_xCoO_3$ ($0 < x < 1$) is well known for samples prepared by traditional high-temperature ($> 800\,^{\circ}C$) calcination [9]. Precursor materials (usually oxides) are mixed and fired for several days with repeated mixing until a constant composition is reached.

Strontium cobalt oxide, $Sr_2Co_2O_5$ forms two phases, the more stable of which has a hexagonal structure and is the only compound in this series previously reported to exhibit vacancy ordering of the type reported here [10]. At the other extreme, lanthanum cobalt oxide, $LaCoO_3$, is rhombohedral with an angle of around 91° [9]. This distortion diminishes with the introduction of strontium, until at $x = 0.5$, the structure is cubic. Up to $x = 0.5$ the structure may respond to strontium substitution by stabilizing Co^{4+} rather than by losing oxygen [9], although we have found that the preparation conditions also determine the oxygen stoichiometry. For $x > 0.5$ oxygen must be lost, but there have been no reports of the effect of this loss on the structure. This is surprising, because vacancy ordering is well known in related compounds such as ferrites [11, 12] and manganites [13, 14]. Earlier studies have shown $BaCoO_{3-y}$ [15] to exhibit at least seven vacancy-ordered phases and, more recently, vacancy ordering has been reported in $MCoO_{3-y}$, where M = Co, La, Sm and Nd [16]. The structure of oxide superconductors with high transition temperatures has been discussed in terms of oxygen-deficient perovskites [17].

Tseung and Bevan [18] showed that rapidly freezing a solution containing a mixture of ions followed by sublimation of the solvent led to the retention of the intimate mixing in the resulting solid, reducing thereby the reaction temperature to around 550 °C and reaction time to 10–20 h. The so-called freeze drying method has been shown to be particularly useful for the preparation of mixed metal oxides when a third step is included; that of vacuum decomposition of the dried precursor salt [19]. Studies of the method [20–22] have concentrated on the factors influencing the drying time and those that ultimately determine surface area. It has been assumed that the structure produced by the method is essentially that arrived at by conventional calcination techniques, but with a product of higher surface area. In the case of strontium-substituted lanthanum cobaltites we have shown this not to be so [23]. In the present study, the effect on the structure of the product of the calcination temperature of the freeze-dried nitrate mixtures, as well as some conditions of the freeze drying method, is reported and evidence is given for vacancy ordering. The changes in electrocatalytic activity with preparation are also detailed.

* *Permanent address*: Department of Metallurgy and Materials Engineering, Ecole Polytechnique, P.O. Box 6079, Station A, Montreal, QC, Canada H3C 3A7.

0022–2461

2. Experimental procedure

2.1. Preparation of compounds

2.1.1. Materials

All chemicals were of analytical reagent grade purity. The exact content of lanthanum, strontium and cobalt in the salts $La(NO_3)_3 \cdot 6H_2O$, $Sr(NO_3)_2$ and $Co(NO_3)_2 \cdot 6H_2O$, respectively, was checked by standard complexometric titration methods. Solutions were made up in deionized, distilled water to 0.5 mol dm^{-3} in cobalt with the other elements as required by stoichiometry. Solutions were filtered before use.

2.1.2. Spray freezing and freeze drying

A solution containing 30–50 cm^3 was rapidly frozen by spraying as a fine mist from a hand-held sprayer into approximately 1 dm^3 liquid nitrogen which was continuously stirred with a glass rod. The free-flowing slurry was poured into a pre-cooled 250 cm^3 round-bottomed flask. This was attached to a glass vacuum apparatus pumped by a rotary pump. A feature of the apparatus is a large liquid nitrogen trap close to the flask into which the water from the sample sublimes. The design and operation of the apparatus have been detailed elsewhere [18, 19]. In this work, heating by an infrared lamp [20] was not used, and for some samples ($x = 0.2$) insulation was necessary to prevent melting. Melting occasionally occurred and this is known to produce an inferior product [18]. After 24–30 h, drying was complete. Complete dehydration and partial decomposition was effected *in situ* by heating with a mantle at 300 °C for about 6 h until the pressure fell below 1 Pa. The resultant powder was black, friable and had a large surface area (about 50 $m^2 g^{-1}$). The samples to be characterized were prepared from the freeze-dried material by calcining in air in a furnace at temperatures between 560 and 1000 °C for different times.

2.2. Characterization

X-ray characterization was performed on a Siemans M34025 diffractometer using CuK_α radiation. The surface area measurements were made by a single-point BET method on a Micrometrics surface area analyser with nitrogen as the adsorbing gas. The conductivity of each sample was determined by measuring the resistance of a pellet compressed to 20 kgf between steel rods in a glass tube of internal diameter 2.5 mm, external diameter 8 mm. Samples were also checked for undecomposed nitrate by differential thermal analysis (DTA).

2.3. Electrochemistry

For electrochemical measurements the powders were compressed at 5 MPa to a disc of 5 mm diameter and 2 mm thickness and heated at 400 °C for 5 h. The disc was located coaxially in a recess in a cylindrical PTFE holder. Electrical contact was made through the back of the holder by silver epoxy resin, which also served to retain the disc. The front surface was polished down to the level of the holder and the electrode assembly was immersed in molten hydrocarbon wax. This filled pores in the disc by capillary rise and protected the backing electrical contact from electrolyte during the experiment. Finally, the front surface was repolished to expose the powder. The electrode assembly was used as a rotating disc working electrode (2000 r.p.m.) in a solution of 5 mol dm^{-3} potassium hydroxide in a glass three-compartment cell. The secondary electrode was a 2 cm × 2 cm platinum foil and a saturated calomel electrode (+ 0.242 V versus SHE) was the reference electrode. The potential was scanned at 20 mV s^{-1} between − 1.0 and + 0.8 V by a PAR Model 1704 potentiostat and Model 1234 signal generator. The current was digitized and stored in an IBM-Xt clone using LABTECH NOTEBOOK software. The cyclic voltammogram was repeated for the potassium hydroxide solution containing 8 mmol dm^{-3} methanol. The percentage difference in current at + 0.4 V was taken as a measure of the ability of the sample to oxidize methanol.

3. Results and discussion

3.1. Preparation

3.1.1. Spray freezing/freeze drying

There are many complex processes that occur in going from a solution of metal nitrates to a final high surface area mixed oxide. In earlier investigations we have shown that the compositions that form the eutectic may melt whatever the initial concentration [19–21]. It is, therefore, of importance to maintain the temperature of the solid below this value by sufficiently fast sublimation during the drying process. The critical times are at the beginning, when the pressure may not be sufficiently low, and at a stage during drying when the rate of sublimation falls due to the reducing surface area of the ice ball, and its coverage with dried product. We found that even a small amount of melting at the sublimation step resulted in lower surface area, lower conductivity and different XRD patterns probably due to inhomogeneous phase formation. We varied the concentration of the solutions between 0.5 and 1.0 mol dm^{-3} in total cation and perceived no difference in the product. We found the finest spray (< 1 mm droplets) giving a mist of solution resulted in the highest surface area, although no systematic study was done on this factor.

3.1.2. Calcination

The vacuum calcination step (heating < 300 °C) gave a black powder that was completely dehydrated and contained no nitrates of cobalt or lanthanum. Strontium nitrate was not decomposed at this stage. XRD patterns gave characteristic sharp peaks of strontium nitrate superimposed on a high rolling background of an amorphous material. DTA showed an endothermic peak at 580 °C as strontium nitrate decomposed. No exothermic peak associated with the formation of a perovskite phase could be seen. This supports the XRD data that showed, for a given composition, a series of patterns as the temperature of calcination was increased from 570 °C to 1050 °C. Up

TABLE I Indexed and fitted XRD pattern of cubic perovskite $La_{0.5}Sr_{0.5}CoO_3$. $a_c = 0.382_3 \pm 0.0006$ nm

d_{obs} (nm)	d_{calc} (nm)	I		hkl
		Measured	Calculated	
0.3810	0.3823	9	6	100
0.2706	0.2703	100	98	110
0.2206	0.2207	16	19	111
0.1914	0.1912	32	34	200
0.1706	0.1710	3	3	210
0.1563	0.1561	28	31	211
0.1352	0.1352	12	16	220
0.1274	0.1274	2	2	221
0.1210	0.1209	10	11	310
0.1154	0.1153	2	4	311
0.1103	0.1104	3	4	222
0.1023	0.1022	9	12	321

to 550 °C the material remained amorphous. It is likely, therefore, that there is not one definite moment at which a given perovskite becomes fully formed from an amorphous precursor, but an evolution through several apparently metastable phases showing different amounts of anion vacancy.

The following sequence of events may be proposed to occur during the freeze-drying/calcination process: (1) dehydration; (2a) decomposition of cobalt nitrate; (2b) decomposition of lanthanum nitrate (> 450 °C); (3) formation of amorphous $LaCo_{1+x}O_{3-y}$ plus Co_3O_4 (ca. 550 °C); (4) decomposition of strontium nitrate (> 550 °C); (5) formation of $SrCoO_{3-y}$ plus a ternary, crystalline (La, Sr, Co oxide) phase (> 570 °C); (6) ordering of ternary oxide phase as the temperature and time of calcination increase; (7) formation of the stoichiometric perovskite structure (> 1000 °C or in higher partial pressure of oxygen). These steps are apparently involved in the process, regardless of the means of homogenization. However, when using freeze-drying, the formation of perovskite takes place at temperatures about 200 °C lower than are required when the oxides are simply mixed, and it is considerably faster. For example, preparation of stoichiometric (cubic) $La_{0.5}Sr_{0.5}CoO_3$ starting from nitrates that have been mixed by hand grinding required 3 days calcination at 1000 °C with regrinding at the end of each day. (The XRD data for this compound are given in Table I.) The temperature and the time required for the formation of a given phase may further be influenced by the composition, i.e. the reactivity of the compounds.

3.2. Characterization

3.2.1. Conductivity and surface area analysis

Values of the conductivity of $La_{1-x}Sr_xCoO_{3-y}$ for $x = 0.2$, 0.5 and 0.8 have been published elsewhere [23]. Typically the conductivity increased with longer and higher temperature calcination. If back melting had occurred, then the conductivity was lower. $La_{1-x}Sr_xCoO_3$, $x = 0.8$, had consistently lower conductivities that were less influenced by the heating regime. The highest recorded conductivity (814 $S\,m^{-1}$) was for $x = 0.5$ calcined at 1000 °C. Compounds at the extremes of x ($x = 1$ and $x = 0$) were not conducting.

The specific surface areas (ssas) of compositions with $x = 0.5$ were consistently between 30 and 40 $m^2\,g^{-1}$ after vacuum heating. These values fell to $< 15\ m^2\,g^{-1}$ on perovskite formation at about 580 °C and then to about $3\ m^2\,g^{-1}$ after calcination at 1000 °C. We have shown that the drop in surface area is exponential with time and that the conductivity increases as this occurs [22].

TABLE II XRD patterns of freeze-dried powders of composition $SrCoO_{2.5}$, subjected to different calcining regimes. The assignments and calculated d values and intensities are for a 2H cell with $a = 0.5471$ nm, $c = 0.4235$ nm

T(°C)/time (h)								
750/10		950/10		1150/10				
d (nm)	I	d (nm)	I	d (nm)	I	d_{calc} (nm)	I_{calc}	hkl
0.4720	15	0.4745	11	0.4745	15	0.4745	12	100
0.3121	48	0.3110	61	0.3143	53	0.3158	59	101
				0.3038	11			
0.2734	100	0.2747	100	0.2730	100	0.2736	85	110
0.2433	6	0.2428	6					
		0.2140	5					
0.2122	5	0.2117	6	0.2120	6	0.2120	4	002
0.2058	36	0.2058	37	0.2060	37	0.2068	50	201
0.1929	8	0.1937	7	0.1933	16	0.1933	27	102
		0.1892	5					
0.1660	5	0.1676	5					
		0.1647	19			0.1649	6	211
0.1621	17			0.1616	7			
				0.1595	13	0.1579	19	202
0.1580	12	0.1583	12	0.1578	15	0.1578	11	300
		0.1556	5					
0.1497	6	0.1501	7	0.1501	6	0.1480		301
0.1427	3							
0.1370	10	0.1371	11	0.1368	13	0.1368	10	220
0.1255	4	0.1255	4	0.1255	4	0.1255		311
0.1152	3	0.1142	5	0.1152	3	0.1152		222

3.2.2. XRD

The patterns were complex and several perovskite-related, anion deficient patterns have been observed. Table I gives an indexed powder pattern of cubic $La_{0.5}Sr_{0.5}CoO_3$ (from a sample calcined at 1000 °C for 3 days with grinding at the end of each day) with fitted intensities. We present the data for the binary oxide $SrCoO_{3-y}$ and three ternary compositions $La_{1-x}Sr_xCoO_{3-y}$ ($x = 0.8$, 0.5, 0.2) in Tables II–V, respectively.

3.2.1.1. $SrCoO_{3-y}$. Only one type of pattern was observed for freeze-dried strontium cobaltite (Table II). It may be indexed to a hexagonal 2H lattice with cell parameters 0.5471 nm and $c = 0.4235$ nm. Grenier *et al.* [10] produced the same phase ($a = 0.544$ nm, $c = 0.424$ nm) from a brownmillerite phase of stoichiometry $Sr_2Co_2O_5$, after annealing in air at > 600 °C. According to Grenier *et al.* [10] the 2H $Sr_2Co_2O_{3-y}$ contained a slight excess of oxygen, i.e. $y < 0.5$. In an attempt to assign all lines we have tried to fit the pattern to a 4H structure by doubling the length of the *c*-axis. However, while the calculated *d*-spacings would agree well with those observed, they are not predicted to have sufficient intensities, even if the cell is constructed with oxygen vacancies to maximize the intensity of *h k l* with odd *l*. Hutchinson and Jacobson have identified a 4H structure in $Ba_{0.1}Sr_{0.9}MnO_{2.96}$ [14]. A 4H structure is formed at high temperatures by $BaMnO_3$, as reported by Gushee *et al.* [24], but it is not the same as the doubled 2H cell and does not fit the experimental pattern for $SrCoO_{3-y}$, $y < 0.5$.

The patterns of the following $La_{1-x}Sr_xCoO_{3-y}$ compositions are more complex and several correspond apparently to a mixture of two or more phases. Fig. 1 gives the XRD of a sample of $La_{0.5}Sr_{0.5}CoO_{3-y}$ after calcining at 750 °C for 1 h. Each composition exhibits its characteristic set of patterns, but some features are common to all three. For example sharp peaks which appear at *d* (nm) = 0.297, 0.283, 0.234, 0.2023, 0.1431, 0.1429, 0.1223, 0.1220, could be due to a metastable phase. The lines are

TABLE III XRD patterns of freeze-dried powders of composition $La_{0.2}Sr_{0.8}CoO_{3-y}$ subjected to different calcining regimes. The indexed patterns in column 3 are: T, a tetragonal phase of $La_{0.5}Sr_{0.5}CoO_{3-y}$ (see Table VI); 2H, the hexagonal phase of $SrCoO_{2.5}$ (see Table II). Entries in bold signify the sharp lines of a metastable tetragonal phase and the assignments in the last column are to an orthorhombic cell $a = 0.7641$ nm, $b = 0.7760$ nm and $c = 1.131$ nm

T(°C)/time (h)				Assignment	*T*(°C)/time (h)								Assignment	
570/16		1000/0.13			650/4		750/1		750/2		800/2			
d (nm)	*I*	*d* (nm)	*I*		*d* (nm)	*I*	*d* (nm)	*I*	*d* (nm)	*I*	*d* (nm)	*I*	d_{calc}	*h k l*
1.2627	6			T	1.1787	2	1.1787	4	1.1786	6			1.1310	001
0.4796	13	0.4822	5	2H	0.4720	5	0.4720	15	0.4720	3	0.4720	10	0.4906	111
		0.3867	5	T,C	0.3850	1	0.3850	3			0.3786	3	0.3770	003
0.3562	10			T			0.3562	13						
				T			0.3453	9	0.3427	3			0.3428	210
0.3351	7			T										
0.3153	60	0.3146	22	2H	0.3132	53	0.3132	54	0.3132	50	0.3110	56	0.3166	202
					0.2973	**2**			**0.2973**	**10**	**0.2973**	**13**		
							0.2849	**3**						
		0.2814	12	T					0.2805	10	0.2805	10	0.2828	004
0.2747	100	0.2743	57	2H										
0.2722	67	0.2719	100	T,C	0.2718	100	0.2722	100	0.2722	100	0.2722	100	0.2722	220
					0.2698	69	0.2698	75	0.2698	67	0.2698	63	0.2704	023
					0.2675	18	0.2675	10	0.2675	14	0.2675	19	0.2683	203
0.2442	13	0.2442	3	T	0.2426	9	0.2426	9	0.2426	10	0.2426	13	0.2420	310
					0.2344	**4**	**0.2344**	**13**	**0.2344**	**14**	**0.2344**	**6**		
					0.2273	4	0.2273	3	0.2273	1	0.2273	3	0.2285	024
0.2222	7	0.2229	12	T	0.2201	4	0.2212	4	0.2209	4	0.2201	9	0.2225	312
0.2129	13	0.2129	3	2H,T	0.2106	6	0.2106	8	0.2106	9	0.2106	6	0.2110	303
0.2076	39	0.2067	15	2H										
0.2053	10	0.2045	7	T	**0.2053**	**32**	**0.2053**	**34**	**0.2053**	**36**	**0.2053**	**34**		
					0.1961	3	0.1961	4	0.1961	4	0.1961	4	0.1961	224
		0.1941	7	2H			0.1936	14	0.1936	16	0.1933	18	0.1940	040
0.1929	25	0.1922	30	T	0.1912	19	0.1914	18	0.1914	20	0.1914	20	0.1910	400
0.1653	14	0.1654	7	2H	0.1645	12	0.1644	14	0.1644	16	0.1645	16	0.1640	422
		0.1588	10	2H	0.1570	13			0.1578	17	0.1570	16	0.1582	017
0.1578	19	0.1568	25	2H	0.1566	15	0.1570	15	0.1566	17	0.1566	16	0.1581	107
0.1503	6	0.1503	3	T	0.1497	6	0.1497	5	0.1497	6	0.1497	5	0.1497	052
0.1437	10	0.1437	3	2H	**0.1433**	**12**	**0.1433**	**75**	**0.1435**	**26**	**0.1433**	**10**		
							0.1431	**44**	**0.1432**	**19**				
0.1373	13	0.1373	5	T	0.1366	12	0.1366	10	0.1366	13	0.1370	9	0.1361	054
0.1359	10	0.1359	12	2H	0.1353	9	0.1353	10	0.1353	7	0.1353	9	0.1355	344
0.1258	3	0.1258	2	2H	0.1254	4	0.1259	4	0.1259	4	0.1254	4	0.1268	426
0.122	10	0.1224	2	T			**0.1222**	**38**	**0.1224**	**13**				
0.121	8	0.1215	7	T	**0.1217**	**5**	**0.1220**	**24**			**0.1217**	**5**		

TABLE IV XRD patterns of freeze-dried samples of composition $La_{0.5}Sr_{0.5}CoO_{3-y}$ subjected to different calcining regimes. Entries in bold arise from a metastable tetragonal phase

T(°C)/time (h)											
570/16		650/4		750/1		750/2		800/2		1000/0.13	
d (nm)	I	d (nm)	I	d (nm)	I	d (nm)	I	d (nm)	I	d (nm)	I
1.2627	6	1.2109	7	1.2109	7	1.2627	8	1.2011	8		
0.5754	4	0.5680	3	0.5673	2	0.5791	14				
0.4796	2	0.4720	1	0.4770	2	0.4822	3	0.4770	3		
						0.3867	7			0.3857	6
0.3834	7	0.3834	7	0.3818	6			0.3834	5		
0.3534	9	0.3534	14	0.3531	2						
0.3453	3	0.3453	8					0.3427	4		
		0.3278	5			0.3290	10				
						0.3220	19				
0.3178	16	0.3175	14	0.3164	4	0.3164	21	0.3143	5		
				0.3121	11			0.3121	13		
		0.2998	3	0.2988	1	0.3028	3	0.2998	6		
				0.2963	**1**			**0.2973**	**19**		
0.2831	**5**	**0.2831**	**5**	**0.2831**	**2**	**0.2823**	**8**	**0.2844**	**5**	**0.2824**	**9**
				0.2797	4			0.2797	13		
0.2725	100	0.2725	100	0.2714	78	0.2730	100			0.2724	100
				0.2698	57			0.2702	100		
0.2458	5	0.2449	5			0.2455	7			0.2462	1
				0.2429	3			0.2429	11		
0.2363	**4**	**0.2356**	**5**	**0.2338**	**22**			**0.2338**	**5**	**0.2365**	**3**
0.2285	4	0.2276	3			0.2298	10	0.2276	3	0.2298	1
0.2221	10	0.2212	7	0.2209	8	0.2227	10	0.2208	13	0.2230	13
						0.2137	3				
										0.2103	2
0.2061	5	0.2061	8	0.2056	7	0.2071	12	0.2056	8		
		0.2036	**3**	**0.2025**	**25**			**0.2025**	**6**	**0.2049**	**3**
		0.1973	4					0.1971	4		
0.1926	26	0.1926	23	0.1914	19	0.1929	26	0.1914	29	0.1926	29
0.1880	4	0.1877	4			0.1884	10				
0.1721	4							0.1713	1	0.1722	2
		0.1759	3								
		0.1670	3			0.1670	7	0.1643	6		
		0.1647	3	0.1654	1						
0.1570	26	0.1570	22	0.1568	17	0.1575	23	0.1562	25	0.1569	24
0.1438	**7**	**0.1435**	**8**	**0.1431**	**100**	**0.1439**	**10**	**0.1431**	**9**	**0.1441**	**11**
				0.1429	**60**						
0.1362	10	0.1361	8	0.1356	6	0.1361	10	0.1352	10	0.1361	10
								0.1258	4		
0.1226	**11**			**0.1223**	**49**	**0.1225**	**5**			**0.1225**	**17**
		0.122	**7**	**0.122**	**28**	**0.122**	**7**	**0.122**	**6**	**0.122**	**9**
0.121	5	0.121	7	0.122	5			0.121	8		

particularly sharp and stand out from the broader patterns. Fig. 2, which gives the XRD of a different sample of $La_{0.5}Sr_{0.5}CoO_{3-y}$ calcined at 750 °C for 1 h, is a good example of the phase. These lines are given in bold in the tables to distinguish them from lines of the indexed phases. The presence of oxygen vacancies which require there to be Co^{2+} for $y > x/2$ indicates that the calcination regimes used were not sufficient for full oxidation of cobalt.

3.2.1.2. $La_{0.2}Sr_{0.8}CoO_{3-y}$. This composition showed the least dependence of the pattern (and hence the structure) on the calcination conditions. Indeed only two distinct patterns were observed. These are given and indexed in columns 1 and 2, and columns 3–6 of Table III. The first patterns are of an intergrowth of two phases, 2H $SrCoO_{2.5}$ and a tetragonal phase of $La_{0.5}Sr_{0.5}CoO_{3-y}$ ($y = 0.25$). The other four patterns, two of which contain the lines of the above described metastable phase do not show a clear presence of the hexagonal $SrCoO_{2.5}$. Rather they seem to fit an orthorhombic structure with $a = 0.7641 \pm 0.0005$ nm, $b = 0.7760 \pm 0.0005$ nm and $c = 1.131 \pm 0.001$ nm.

3.2.1.3. $La_{0.5}Sr_{0.5}CoO_{3-y}$. The patterns for this composition are presented in Table IV and show the evolution of a tetragonal phase with $a = 2a_c$ (a_c is the unit cell parameter of the cubic $La_{0.5}Sr_{0.5}CoO_3$) and $c = 3a$. The pattern of the metastable phase (also seen in $x = 0.8$) was observed in some XRDs (see Fig. 2 and Table IV).

The positions and relative intensities of lines of a freeze-dried sample prepared by Anderton and Sale [25] may all be found in the pattern of our sample calcined at 1000 °C for 10 min. Our pattern also agrees

TABLE V XRD patterns of freeze-dried powders of composition $La_{0.8}Sr_{0.2}CoO_{3-y}$, subjected to different calcining regimes. Entries in bold arise from a metastable tetragonal phase

T(°C)/time (h)													
570/16		570/32		650/4		750/1		750/2		800/2		1000/0.13	
d (nm)	I	d (nm)	I	d (nm)	I	d (nm)	I	d (nm)	I	d (nm)	I	d (nm)	I
1.2109	15	1.1946	10			1.2109	8	1.1334	2	1.1787	4		
0.5609	1	0.5609	< 1	0.5609	1	0.5680	17	0.5553	5			0.5717	6
0.4623	3												
0.3818	5	0.3818	5	0.3818	7	0.3834	13	0.3834	35	0.3786	13	0.3867	43
0.3414	17	0.3414	9	0.3414	13	0.3427	3	0.3389	10	0.3376	9	0.3293	4
0.3267	2	0.3267	< 1	0.3267	1	0.3261	14	0.3232	11			0.3202	7
0.3153	3	0.3153	< 1	0.3153	8	0.3187	21	0.3153	18			0.3180	2
0.3048	12			0.3048	8					0.3043	6	0.3028	2
0.2973	**42**	**0.2978**	**18**	**0.2973**	**46**	**0.2988**	**9**	**0.2940**	**13**	**0.2963**	**33**		
0.2830	**2**	**0.2830**	**1**	**0.2830**	**2**	**0.2814**	**8**			**0.2831**	**3**	**0.2831**	**17**
								0.2797	3	0.2792	4		
0.2708	100	0.2722	58	0.2722	50	0.2710	100	0.2690	100	0.2694	100	0.2729	100
				0.2709	100			0.2675	95	0.2671	79	0.2716	93
0.2429	14	0.2429	8	0.2429	12	0.2432	10	0.2417	10	0.2426	7	0.2451	4
0.2344	**23**	**0.2344**	**77**	**0.2344**	**13**	**0.2350**	**6**	**0.2332**	**2**	**0.2327**	**2**	**0.2367**	**1**
0.2276	14	0.2276	5	0.2276	15	0.2287	15	0.2259	17	0.2265	8	0.2297	4
0.2201	12	0.2201	5	0.2206	13	0.2217	14	0.2201	17	0.2203	18	0.2230	19
										0.2171	3	0.2203	6
						0.2146	4	0.2127	3			0.2103	2
0.2023	**21**	**0.2025**	**58**	**0.2023**	**13**	**0.2032**	**5**	**0.2014**	**3**	**0.2019**	**2**	**0.2053**	**4**
0.1961	**20**	**0.1973**	**5**	**0.1969**	**15**	**0.1973**	**5**	**0.1957**	**5**	**0.1961**	**8**		
0.1922	26	0.1922	18	0.1922	27	0.1914	32	0.1899	38	0.1907	40	0.1926	50
0.1877	5			0.1863	6	0.1870	13	0.1857	13			0.1881	4
0.1755	9	0.1755	2	0.1755	10	0.1759	1	0.1746	< 1	0.1746	9	0.1726	4
						0.1707	5			0.1713	3		
0.1701	5			0.1696	6			0.1698	3	0.1698	3		
0.1645	15	0.1645	5	0.1656	12	0.1670	6	0.1656	5	0.1650	7		
										0.1636	5		
0.1563	30	0.1563	14	0.1563	27	0.1568	27	0.1561	33	0.1562	29	0.1572	33
										0.1549	11	0.1558	9
										0.1488	2		
0.1431	**76**	**0.1431**	**100**	**0.1431**	**29**	**0.1435**	**11**	**0.1425**	**5**	**0.1431**	**3**	**0.1438**	**6**
0.1429	**45**	**0.1429**	**70**	**0.1429**	**23**					**0.1423**	**3**		
0.1368	6	0.1368	8			0.1364	8	0.1358	12	0.1358	10	0.1363	7
0.1361	10	0.1361	8	0.1358	10	0.1351	8	0.1344	12	0.1347	8	0.1354	9
0.1259	5			0.1259	2					0.1258	3	0.1282	2
0.1225	**20**	**0.1225**	**100**	**0.1224**	**44**	**0.1225**	**6**					**0.1225**	**4**
		0.1223	**67**	**0.1222**	**39**			**0.1220**	**8**			**0.1218**	**7**
0.1215	10	0.1215	12	0.1215	10	0.1212	8	0.1211	8	0.1209	10	0.1212	9

with a pattern quoted by Anderton and Sale as being of commercially prepared $La_{0.5}Sr_{0.5}CoO_3$. We note that both of these patterns (and extra lines found in our pattern and given in Table IV) indicate that the cubic perovskite is not solely present and that a tetragonal distortion must be invoked to index all lines observed.

The lines may be indexed to a tetragonal cell with $a \approx 2a_c = 0.7703 \pm 0.0005$ nm and $c \approx 3a = 2.307 \pm 0.001$ nm as given in Table VI. This model structure corresponds to oxygen vacancies at $z = 0.25$, and 0.75 in a structure that has twelve layers, alternating CoO_2 and (La, Sr)O. The doubling of the a-axis arises from ordering of lanthanum and strontium, and the pattern of oxygen vacancies gives the greater c-axis.

Such a distortion arising from the loss of one mole of oxygen from a three-layer perovskite (i.e. giving $A_3B_3O_8$) has been observed by Rodrigues-Carvajal *et al.* [26] in $Ca_3Fe_2TiO_8$ and $Ca_3Fe_2TiO_8$, and by Grenier *et al.* in $Ca_2LaFe_3O_8$ [27] and in $Ca_3(Mn, Fe)_3O_8$ [28]. The sequential loss of oxygen from $YBa_2Cu_3O_9$ to $YBa_2Cu_3O_8$, $YBa_2Cu_3O_7$, and $YBa_2Cu_3O_6$ was discussed by Galy *et al.* [17] in terms of the tetragonal structures that are produced. Katsuyana *et al.* [29] have reported orthorhombic and tetragonal $YBa_2(Cu_{1-x}Fe_x)_3O_y$ for $0 < x < 0.15$. The orthorhombic form has cell parameters $a = 0.3833$ nm, $b = 0.3876$ nm and $c = 1.168$ nm. The distortion is caused by different oxygen occupancy of the a- and b-sites. As the temperature of annealing increases disordering of oxygen from b-sites to vacant a-sites occurs with loss of oxygen giving the tetragonal form with cell parameters $a = 0.3861$ nm, $c = 1.1670$ nm.

We note that the patterns of samples that partially melted during the drying period showed the presence of unreacted La_2O_3 when calcined at temperatures below 750 °C.

3.2.1.4. $La_{0.8}Sr_{0.2}CoO_{3-y}$. The patterns of the lanthanum-rich composition are collected in Table V.

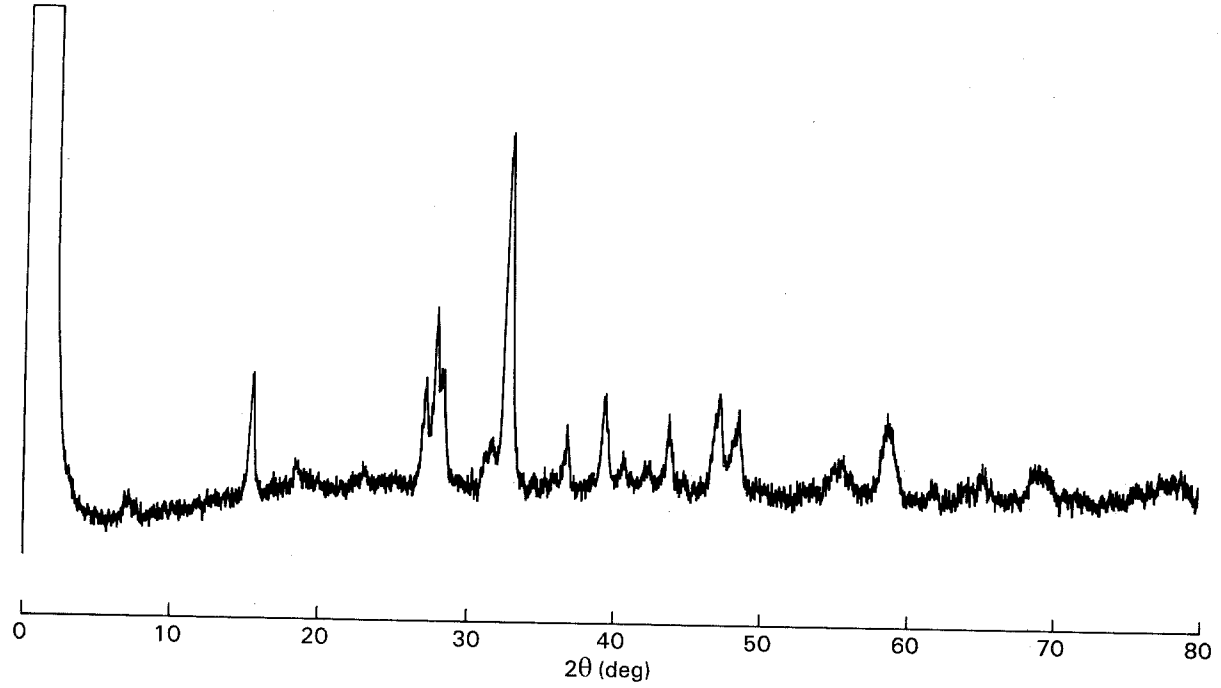

Figure 1 Powder X-ray diffraction pattern of $La_{0.5}Sr_{0.5}CoO_3$ after calcining for 1 h at 750 °C.

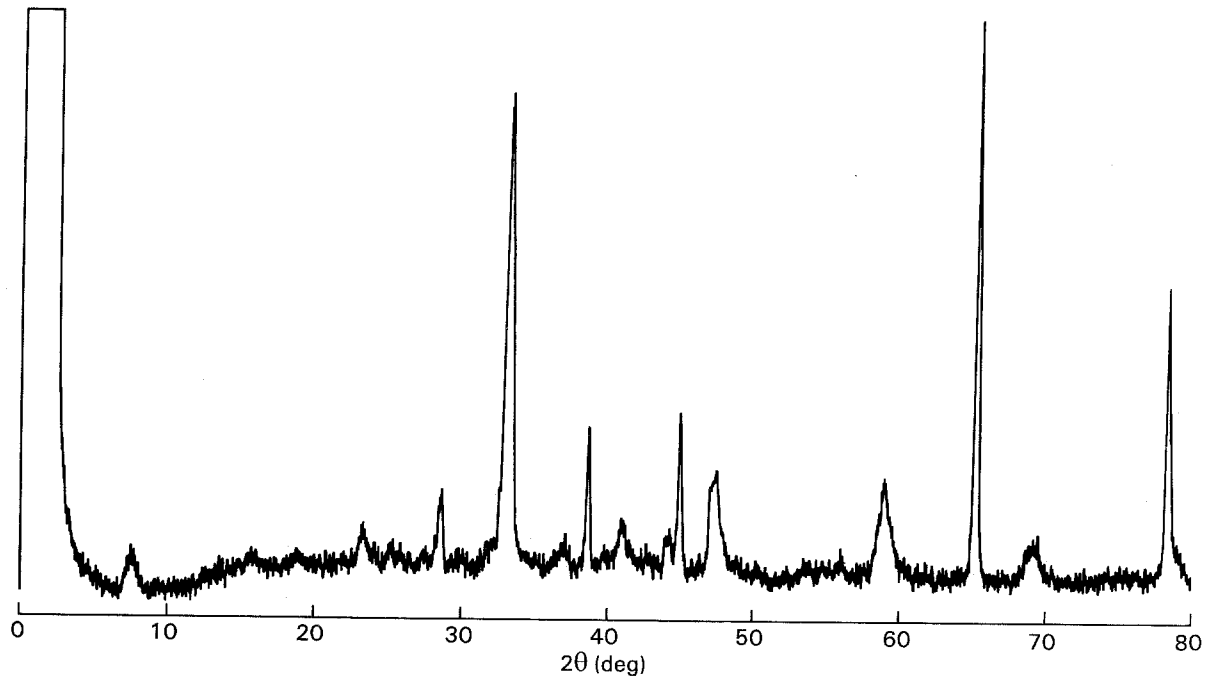

Figure 2 Powder X-ray diffraction pattern of second sample of $La_{0.5}Sr_{0.5}CoO_3$ after calcining for 1 h at 750 °C.

The structures appeared to exhibit a high dependence on the calcination regime with at least four different patterns observed that represent two or more phases each. Again these phases are most likely to be related to ordering of oxygen vacancies.

The lines of the sample calcined at 1000 °C for 10 min may be indexed to an intergrowth of a tetragonal phase similar to that of $La_{0.5}Sr_{0.5}CoO_{3-y}$ ($y = 0.25$) with $a = 0.7719 \pm 0.0005$ nm and $c = 2.296 \pm 0.001$ nm, and a hexagonal phase with $a = 0.5465 \pm 0.0005$ nm and $c = 1.326 \pm 0.001$ nm (see Table VII). We note the similarity of our hexagonal phase to that reported for $La_{0.9}Sr_{0.1}CoO_{3-y}$ by Ohbayashi *et al.* [30] who index their pattern to a hexagonal cell with $a = 0.545$ nm and $c = 1.3152$ nm.

Overall, the presented XRD patterns of the studied compositions indicate that the stoichiometric perovskite-related phases are not formed spontaneously but rather through an evolution of several oxygen-deficient phases. The rate-determining step in producing this phase could well be the oxidation of Co^{2+} and Co^{3+} to Co^{4+}.

3.3. Electrochemical measurements

The cyclic voltammograms of electrodes of the different samples in 5 mol dm^{-3} potassium hydroxide were broad and rather featureless, but did show a slow oxidation and reduction couple that we ascribe to oxidation and reduction of lattice cobalt (Fig. 3). The

TABLE VI Indexed XRD pattern of a tetragonal phase of freeze-dried $La_{0.5}Sr_{0.5}CoO_{2.75}$ from sample calcined at 1000 °C for 10 min. Unit cell dimensions: $a = 0.7703$ nm, $c = 2.307$ nm. Lines in bold arise from the metastable tetragonal phase (see text)

d_{obs} (nm)	d_{calc} (nm)	I		hkl
		Measured	Calculated	
0.3867	0.3852	7	4	200
0.2831	**0.2820**	**13**		
0.2722	0.2723	100	98	220
0.2455	0.2463	3	2	224
0.2362	0.2381	6	5	217
0.2222	0.2222	13	18	226
0.2151	0.2136	1	1	320
0.2103	0.2101	1	6	322
0.2053	0.2056	4	2	219
0.1929	0.1926	33	36	400
0.1568	0.1568	29	29	418
0.1437	**0.1436**	**9**		
0.1359	0.1362	14	11	440
0.1279	0.1280	4	1	258
0.1225	**0.1226**	**3**		
0.1215	0.1216	3	6	621

TABLE VII XRD pattern of freeze-dried $La_{0.8}Sr_{0.2}CoO_{3-y}$ calcined at 1000 °C for 10 min, indexed to an intergrowth of a hexagonal cell $a = 0.5465$ nm, $c = 1.3264$ nm and tetragonal cell $a = 0.7719$ nm, $c = 2.296$ nm

Observed	Hexagonal index		Tetragonal index	
d (nm)	d (nm)	hkl	d (nm)	hkl
0.5717			0.5738	004
0.3867	0.3852	012	0.3860	200
0.3293			0.3279	007
0.3202			0.3202	204
0.3180			0.3147	213
0.3028			0.3023	017
0.2831			0.2811	117
0.2729	0.2733	110	0.2729	220
0.2716	0.2716	014	0.2717	206
0.2451			0.2464	224
0.2367			0.2377	217
0.2297			0.2302	208
0.2230	0.2229	202	0.2222	226
0.2203	0.2211	006	0.2206	218
0.2103			0.2105	322
0.2053			0.2051	219
0.1926	0.1926	204	0.1930	400
0.1881			0.1872	410
0.1726	0.1727	212	0.1723	406
0.1572	0.1574	214	0.1568	418
0.1558	0.1557	117		
0.1363	0.1366	220	0.1365	440
0.1354	0.1356	305	0.1359	508
0.1282	0.1284	306	0.1282	258
0.1212	0.1212	307	0.1213	622

oxidation wave lies just before the onset of oxygen evolution and is at the same potential as a more obvious peak in the cyclic voltammogram of the spinel $NiCo_2O_4$ [31]. The presence of oxygen had no effect on the waves, neither did increasing the rotation speed of the rotating disc electrode. Some samples showed peaks arising from breakthrough of the electrolyte to the silver-loaded epoxy resin beneath. The results from such samples have not been included in the data

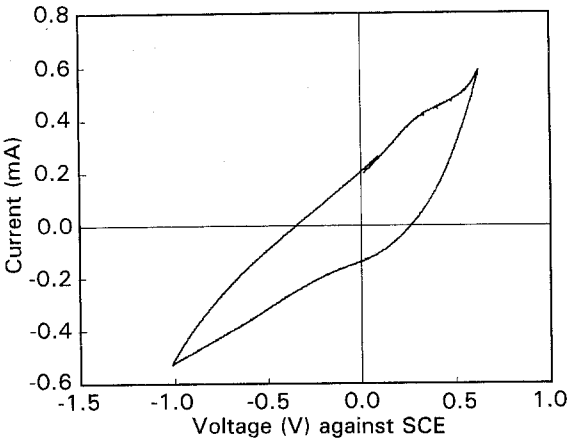

Figure 3 Cyclic voltammogram of a $La_{0.5}Sr_{0.5}CoO_3$ rotating disc electrode (2000 r.p.m.) in 5 mol dm^{-3} KOH at 20 °C. Electrode prepared after calcining at 750 °C for 2 h.

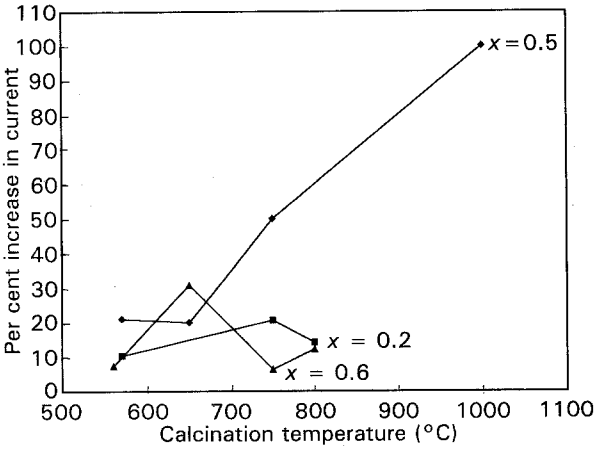

Figure 4 Plot of the percentage increase in current versus calcination temperature of $La_{0.5}Sr_{0.5}CoO_3$ rotating disc electrodes (2000 r.p.m.) when oxidizing a solution of 0.008 mol dm^{-3} methanol at + 0.4 V versus SCE in 5 mol dm^{-3} KOH at 20 °C.

reported here. The addition of methanol led to a general increase in oxidation current and we have used the ratio of the oxidation current with and without methanol to assess the catalytic activity of the electrode. In this way we hope to negate variation from electrode to electrode, due to changes in resistance or other artefacts of fabrication. These are shown in Fig. 4. $La_{0.5}Sr_{0.5}CoO_{3-y}$ is the most active with the activity increasing as the calcination time and temperature increases.

Both $La_{0.8}Sr_{0.2}CoO_{3-y}$ and $La_{0.2}Sr_{0.8}CoO_{3-y}$ gave maxima. It is tempting to suggest that the presence of vacancies in structures that have become sufficiently conducting to have a reasonable activity (note that the conductivities of these compounds were consistently lower than that of $La_{0.5}Sr_{0.5}CoO_{3-y}$) can confer extra catalytic activity. However, the number of samples is limited and the oxidation of methanol may not be representative. We also note that the structure of some samples of $La_{0.2}Sr_{0.8}CoO_{3-y}$ could be interpreted as an intergrowth of $La_{0.5}Sr_{0.5}CoO_{3-y}$ and $Sr_2Co_2O_5$ and so the activity may be related to the amount of the active perovskite and the conductivity of the matrix in which it finds itself. Grenier and

Pouchard [32] tested $La_{1-x}Sr_x(Fe^{3+}_{1-z}Fe^{4+}_z)O_{3-y}$ for the electrochemical reduction of oxygen. The best performance was achieved with $x = 0.95$ and $y = 0.275$ when the amount of oxygen vacancies was at a maximum and the filling of e_g orbitals at a minimum. The reduction of oxygen is thought to proceed via oxidation/reduction mechanisms involving surface O^{2-} and vacancies and these observations are consistent with this view. The mechanism of the oxidation of methanol is less established, but certainly involves adsorbed fragments such as C–OH or HCO. How these would fare on a surface with oxygen vacancies is not so obvious.

4. Conclusion

Freeze drying permits the preparation of well-crystallized perovskite-related phases by calcination at temperatures as low as 580 °C and for relatively short times (< 24 h). Under these conditions a variety of distorted (perovskite) phases is produced. It is suggested that the unit cells of greater size that are observed, many with tetragonal or orthorhombic distortion, arise from oxygen vacancies. For $La_{0.5}Sr_{0.5}CoO_{3-y}$ the catalytic activity towards the oxidation of methanol is a maximum at the cubic perovskite. $La_{0.8}Sr_{0.2}CoO_{3-y}$ and $La_{0.2}Sr_{0.8}CoO_{3-y}$ go through a maximum at a more distorted structure.

References

1. G. H. JONKER, *Physica* **22** (1956) 1118.
2. P. M. RACCAH and J. B. GOODENOUGH, *J. Appl. Phys.* **39** (1968) 1209.
3. R. J. H. VOORHOEVE, D. W. JOHNSON, J. P. RAMEIKA and P. K. GALLAGHER, *Science* **195** (1977) 4281.
4. S. TRASATTI, "Electrodes of Conducting Metallic Oxides" (Elsevier Scientific, Amsterdam, 1980) p. 261.
5. L. G. TEJUCA, J. L. G. FIERRO and J. M. D. TASCON, "Advances in Catalysis", Vol. 36, edited by D. D. Eley, H. Pines and O. B. Weisz (Academic Press, New York, 1989) p. 237.
6. T. NAKAMURA, M. MISONO and Y. YONEDA, *J. Catal.* **83** (1983) 151.
7. D. B. HIBBERT and R. H. CAMPBELL, *Appl. Cat.* **41** (1989) 1988.
8. J. G. BEDNORZ and K. A. MULLER, *Z. Phys. B* **64** (1986) 189.
9. H. L. YAKEL, *Acta Crystallogr.* **8** (1955) 394.
10. J-C. GRENIER, S. GHODBANE, G. DEMAZEAU, M. POUCHARD and P. HAGENMULLER, *Mater. Res. Bull.* **14** (1979) 831.
11. M. A. ALARIO-FRANCO, J-C. JOUBERT and J-P. LEVY, *ibid.* **17** (1982) 733.
12. J. M. GONZALEZ CALBERT, M. VALLET-REGI and M. A. ALARIO-FRANCO, *ibid.* **18** (1983) 285.
13. A. J. JACOBSON and A. J. W. HORROX, *Acta Crystallogr.* **B32** (1976) 1003.
14. J. L. HUTCHISON and A. J. JACOBSON, *J. Solid State Chem.* **20** (1977) 417.
15. M. ZANNE, A COURTOIS and C. GLEITZER, *Bull Soc. Chem. France, Issue* 12 (1972) 4470.
16. T. ARAKAWA, N. OHARA and J. SHOIKAWA, *J. Mater. Sci.* **21** (1986) 1824.
17. J. GALY, R. ENJALBERT, P. MILLET, C. FAULMANN and P. CASSOUX, *J. Solid State Chem.* **74** (1988) 356.
18. A. C. C. TSEUNG and H. L. BEVAN, *J. Mater. Sci.* **5** (1970) 604.
19. *Idem, Electroanal. Chem. Interfacial Electrochem.* **45** (1973) 429.
20. J. KELLY, D. B. HIBBERT and A. C. C. TSEUNG, *J. Mater. Sci.* **13** (1978) 1053.
21. D. B. HIBBERT and A. C. C. TSEUNG, *ibid.* **14** (1979) 2665.
22. D. B. HIBBERT, J. LOVEGROVE and A. C. C. TSEUNG, *ibid.* **22** (1987) 3755.
23. J. KIRCHNEROVA and D. B. HIBBERT, *Mater. Res. Bull.* **25** (1990) 585.
24. B. E. GUSHEE, L. KATZ and R. WARD, *J. Am. Chem. Soc.* **79** (1957) 5601.
25. D. V. ANDERTON and F. R. SALE, *Powder Metall.* **2** (1979) 8.
26. J. RODRIGUES-CARVAJAL, M. VALLET-REGI and J. M. GONZALEZ CALBERT, *Mater. Res. Bull.* **24** (1989) 423.
27. J. C. GRENIER, J. DARRIET, M. POUCHARD and P. HAGENMULLER, *ibid.* **11** (1976) 1219.
28. J-C. GRENIER, F. MENIL, M. POUCHARD and P. HAGENMULLER, *ibid.* **12** (1977) 79.
29. S. KATSUYAMA, Y. UDEA and K. KOSUGE, *ibid.* **26** (1989) 153.
30. H. OHBAYASHI, T. KUDO and T. GEJO, *Jpn J. Appl. Phys.* **13** (1974) 1.
31. D. B. HIBBERT, A. C. C. TSEUNG and P. RASIYAH, *J. Electrochem. Soc.* **129** (1982) 1724.
32. J. C. GRENIER and M. POUCHARD, *Rev. Chim. Mineral.* **21** (1984) 692.

Received 16 June 1992
and accepted 20 April 1993